Aggressive RF Circuit Reduction Techniques in Millimeter Wave Cellular Systems

Abbasi, Muhammad Ali Babar; Tataria, Harsh; Fusco, Vincent F ; Matthaiou, Michail; Alexandropoulos, George C

Published in:
2019 16th International Symposium on Wireless Communication Systems (ISWCS)

DOI:
10.1109/ISWCS.2019.8877347

2019

Document Version:
Peer reviewed version (aka post-print)

Aggressive RF Circuit Reduction Techniques in Millimeter Wave Cellular Systems

M. Ali Babar Abbasi*, Harsh Tataria†, Vincent F. Fusco*, Michail Matthaiou*, and George C. Alexandropoulos‡
*Institute of Electronics, Communications and Information Technology (ECIT), Queen's University Belfast, Belfast, U.K.
†Department of Electrical Engineering, Lund University, Lund, Sweden.
‡Department of Informatics and Telecommunications, National and Kapodistrian University of Athens, Greece
e–mail: {m.abbasi, v.fusco, m.matthaiou}@qub.ac.uk, harsh.tataria@eit.lth.se and alexandg@di.uoa.gr

***Abstract*—In this paper, we introduce a novel hybrid multiuser multiple–input multiple–output (MU–MIMO) architecture, with an emphasis on aggressive millimeter–wave (mmWave) hardware reduction methods, *omitting* the beam selection stage. We propose a simplification in a 28 GHz Rotman lens, where the number of its beam–ports are reduced relative to the array ports resulting in the removal of a bank of RF switches and associated biasing network. We conducted full electromagnetic (EM) characterization of imperative lens defects and precisely quantify the expected loss. For the first time, it is shown that the beam–port decimation greatly *reduces* the total EM aberrations, and consequently *increases* the focusing capability of the lens. With maximum–ratio (MR) baseband processing, we study uplink signal–to–interference–plus–noise of user terminal, and evaluate the sum spectral efficiency performance of the proposed system assuming a 28 GHz double–directional propagation channel. The performance of the proposed system is compared with the classical system including the beam selection network. Although the performance of the proposed architecture is sub–optimal relative to the conventional case, we demonstrate that it greatly simplifies the practical realization of the mmWave RF front–ends, while still maintaining highly desirable and useful operational characteristics.**

I. Introduction

Millimeter wave (mmWave) carrier frequencies will be an integral component the 5G mobile communication systems as per Release 15 standardization by the Third Generation Partnership Project–New Radio (3GPP–NR) [1]. MmWave front–end systems still face a number a technical challenges which need to be resolved before a large–scale deployment [2]. One of the most important technical challenges in mmWave communication is the path–loss. To effectively project a signal over moderate distances and to close the communication link budget, mmWave systems need high gain radiators. This is generally realized by 32 to 256 antenna elements arrays at the cellular base–station (BS) [1]). Since a stand alone array is capable of beamforming only along the broad–side direction, *electronic beam steering* is very much required for spatial sectoral coverage. This requires a *phase–shifter* per antenna element, which needs to be connected to a *dedicated* up/down–conversion radio–frequency (RF) transceiver for conventional multiple–input multiple–output (MIMO) realization. The implementation of such a system with large number of antenna elements is not easy at mmWave frequencies, primarily because of the overall hardware cost. A number of studies have focused on reducing the number of RF chains by carefully devising hybrid architecture where the MIMO system process is shared by the RF front–end and the baseband signal processing (SP) unit [3, 4]. Nevertheless, almost all hybrid architectures suggest *sharing* RF front–end equipment including phase–shifters. Realizing this, again, is complicated primarily because the varactor–controlled phase–shifter at mmWave have high insertion loss which depends upon the control voltage. Connecting multiple phase–shifters requires a dedicated biasing network and are generally not feasible over wide mmWave bandwidths. Efforts like [5] have tried to increase the accuracy by using novel tunable materials, but at expense of high fabrication cost. A lucerative alternative of phase–shifters used in a number of recent hybrid architectures is the *RF lens* [6–11]. In the context of mmWave cellular systems, an ideal RF lens performs the *power combining*, and *phase shifting* at the same time by using the physical principles of electromagnetic (EM) energy focusing. As a result, they reduce the implementation complexity of RF front–ends multi-fold, compared to phase–shifter–based hybrid solutions.

Contributions. A 28 GHz hybrid beamforming architecture for multiuser MIMO (MU–MIMO) operation with an emphasis to reduce the required RF complexity is proposed. Unlike most previous works, we consider the practical anomalies within a Rotman lens with an aid of full–wave electromagnetic (EM) simulations using finite–difference time domain (FTDT) numerical method. Our investigation involves a Rotman lens with $L = M = 13$ (see Fig. 1), and a decimated beam–ports Rotman lenses with $L = 7$ and $M = 13$. We consider a practical uniform linear array (ULA) connected to Rotman lens in receive mode, and precisely quantified the defects of the lens in terms of *spillover* of the EM energy [12]. Based on the simulations, we conclude that the spillover profile at the beam–ports is highly sensitive to the incoming EM signal's direction–of–arrival (DOA). The amount of spillover is significantly higher for DOAs close to the array end–fire, where EM reflections skew the spillover profiles. We also find out that decimating the beam–ports from 13 to 7 significantly reduces the amount of spillover, since every second beam–port is removed; consequently, the electrical distance between consecutive beam–ports gets larger. As a result, this is beneficial in reducing the net RF interference. We carefully characterize the trade–offs in the signal–to–interference–plus–noise ratio (SINR) and sum spectral efficiency by removing the RF switch from the conventional hybrid architecture, and list its fundamental implications from a system implementation point of

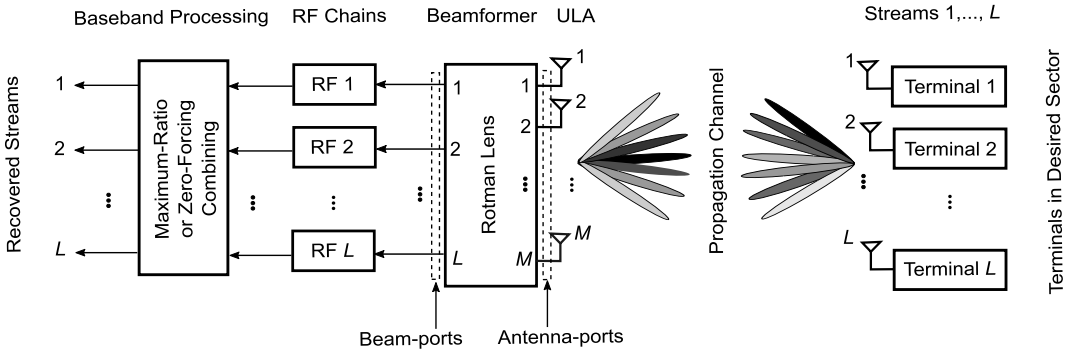

Fig. 1. Proposed hybrid uplink MU–MIMO system using a Rotman lens as the analog beamformer and MRC baseband processing.

view. We employ maximum ratio combining (MRC) baseband processing on the uplink of a MU–MIMO system (see Fig. 1). To facilitate a more accurate comparison with the classical architecture, we devise a model for circuit imperfections in the RF switching stage, by capturing the physical impairments of poor port isolation and impedance mismatches.

II. System Model and Hardware Design

The system model in this work is analogous to the one described in [9] where a typical uplink of a single cell, multiuser system is considered, where the BS is equipped with an M element ULA. The BS receives L separate data streams from L non–cooperative single–antenna terminals ($L \ll M$) within the same time–frequency resource. The terminals are uniformly distributed within a discrete sector of 100°, with a radius of R_{sector}. We let the M fixed analog beams in the azimuthal directions $\phi_1, \phi_2, \ldots, \phi_M$. Then, the $L \times 1$ dimension–reduced signal after beam selection is given by

$$\mathbf{y} = \rho_{\text{t}}^{\frac{1}{2}}\, \mathbf{S}_{\text{RF}}\, \mathbf{F}_{\text{RF}}\, \mathbf{H}\mathbf{x} + \mathbf{n} = \rho_{\text{t}}^{\frac{1}{2}}\, \mathbf{G}\mathbf{x} + \mathbf{n}, \tag{1}$$

where $\mathbf{G} = [\mathbf{g}_1\ \mathbf{g}_2\ \ldots \mathbf{g}_L]$ is an $L \times L$ matrix such that the $L \times 1$ vector $\mathbf{g}_\ell = \mathbf{S}_{\text{RF}}\, \mathbf{F}_{\text{RF}}\, \mathbf{h}_\ell$, $\forall \ell = 1, 2, \ldots, L$. Further details of the system and mathematical definitions can be found in [9]. The net functionality of an ideal Rotman lens with perfect focusing capability is described by the $M \times M$ matrix, $\mathbf{F}_{\text{RF}}$, such that

$$\mathbf{F}_{\text{RF}} = \left[\mathbf{a}^H(\phi_1)\ \ \mathbf{a}^H(\phi_2)\ \ \ldots\ \ \mathbf{a}^H(\phi_M)\right]^T. \tag{2}$$

Where $\mathbf{a}$ is the complex array steering vector and $(\cdot)^H$ is the Hermitian operation. With a perfect switching matrix, $\mathbf{S}_{\text{RF}}$ is an $L \times M$ binary matrix and each row of it contains only one non–zero entry corresponding to the selected beam port index. The $L \times 1$ vector of additive Gaussian noise is denoted by $\mathbf{n}$, where each entry of $\mathbf{n} \sim \mathcal{CN}(0, 1)$. We denote the imperfect switching matrix as $\widetilde{\mathbf{S}}_{\text{RF}} = \mathbf{S}_{\text{RF}} + \mathbf{\Xi}$, where the (r, s)–th entry of $\mathbf{\Xi}$, denoted by $[\mathbf{\Xi}]_{r,s} = e_{r,s} \sim \mathcal{CN}(0, \sigma_{\text{E}}^2)$. Here, σ_{E} controls the level of return loss.

We realize a 28 GHz Rotman lens is on Taconic-RF 60 substrate with dielectric constant $\epsilon_{\text{r}} = 6.15$, $h = 0.64$ mm and dissipation factor $\tan(\delta) = 0.0038$ using *microstrip* technology. The *Wave Medium Propagation* section (see [9]) of the Rotman lens was first synthesized using the standard trifocal lens architecture [13, 14] with $f_1 = 5\lambda$ hosting 13 beam–ports and 2 dummy ports. From here, we design two separate lens configurations, first with array ports $L = M = 13$ (namely 13×13 lens) and then with $L = 7$ and $M = 13$ (namely 7×13 lens). The (r, s)–th element of the imperfect Rotman lens matrix, $\widetilde{\mathbf{F}}_{\text{RF}}$, can be denoted by

$$[\widetilde{\mathbf{F}}_{\text{RF}}]_{r,s} = \tilde{f}_{r,s} = \left(\widetilde{\mathbf{a}}_r^H\right)_s = \underbrace{N^{-\frac{1}{2}}\, e^{-jk_0(s-1)\Delta \sin(\phi_r)}}_{\text{Perfect component, } (\mathbf{a}_r^H)_s\, =\, f_{r,s}}\, e^{j\delta_{r,s}}, \tag{3}$$

where $\delta_{r,s} \sim \mathcal{CN}(0, \epsilon^2)$, and ϵ controls the level of spillover loss and $\widetilde{\mathbf{a}}_r$ is the shorthand for $\widetilde{\mathbf{a}}(\phi_r)$.

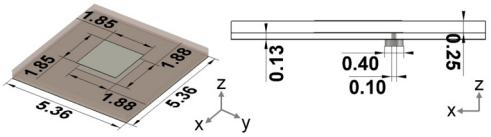

Fig. 2. Geometrical configuration of ULA unit cell (dimensions are in mm).

To realize a non–ideal ULA, first, we designed an antenna unit cell structure consisting of a coax fed microstrip patch printable on two sides of a single Rogers RT/duroid 6006 laminate. An additional patch is printed on another layer, specifically designed to enhance the antenna performance and gain in a wide bandwidth [15, 16]. The geometrical parameters of antenna are shown in Fig. 2. we replicate the same unit cell in a 13 element ULA formation. Lens and arrays with high precision full-wave EM simulations are expected to match the hardware measurements as previously been verified [18, 19]. With MRC at the BS and noise variance of σ^2, the SINR of terminal ℓ with an imperfect lens and RF switching matrix is given by

$$\text{SINR}_\ell = \frac{\rho_{\text{t}} \left|\widetilde{\mathbf{g}}_\ell^H \widetilde{\mathbf{g}}_\ell\right|^2}{\sigma^2 \widetilde{\mathbf{g}}_\ell^H \widetilde{\mathbf{g}}_\ell + \rho_{\text{t}} \sum\limits_{\substack{i=1 \\ i \neq \ell}}^{L} \left|\widetilde{\mathbf{g}}_\ell^H \widetilde{\mathbf{g}}_i\right|^2}. \tag{4}$$

For a given instance of $\widetilde{\mathbf{g}}_\ell$ and $\widetilde{\mathbf{g}}_i$, SINR_ℓ can be translated into an instantaneous spectral efficiency (in bit/sec/Hz) for terminal ℓ via $\text{R}_\ell = \log_2(1 + \text{SINR}_\ell)$. This can be used to compute the ergodic sum spectral efficiency of the system via

$$\text{R}_{\text{sum}} = \sum_{\ell=1}^{L} \text{R}_\ell. \tag{5}$$

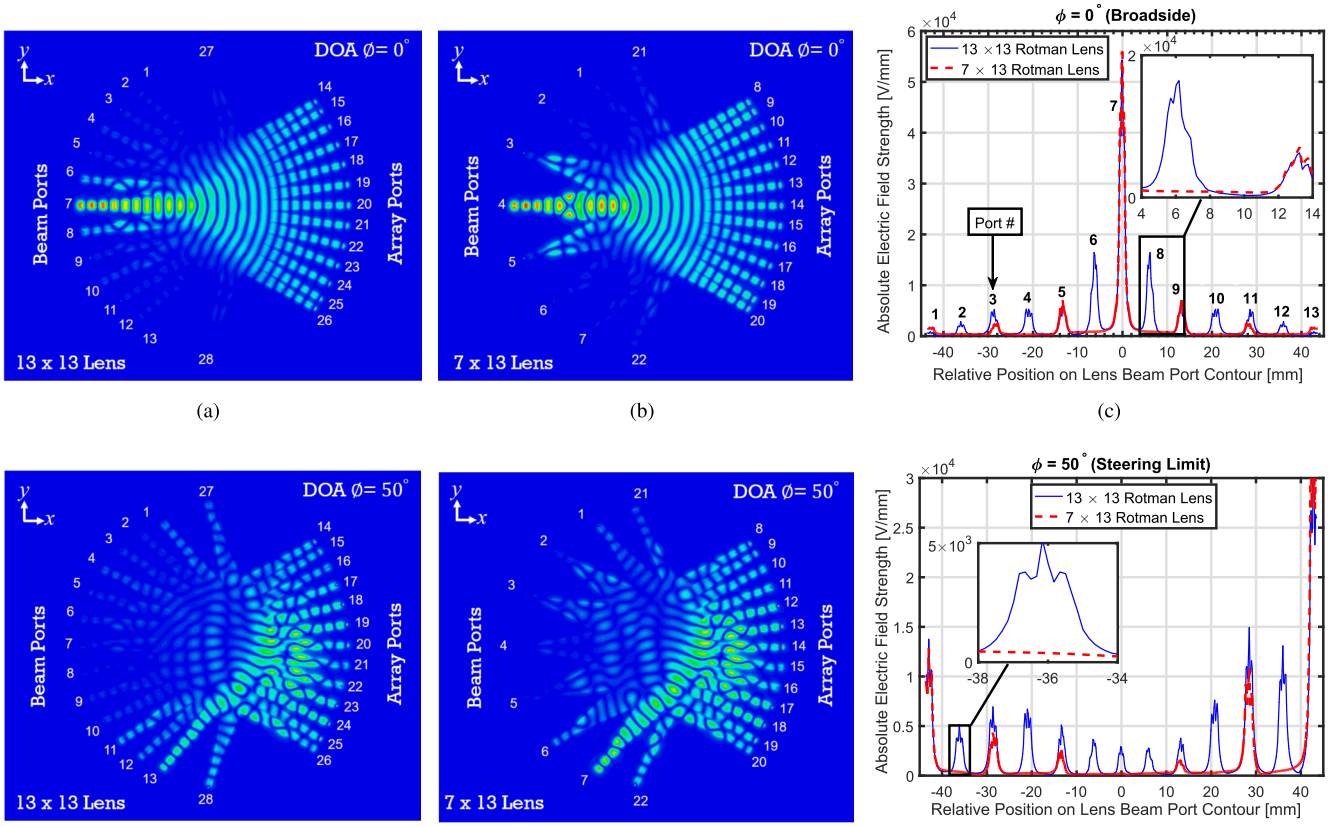

Fig. 3. Simulated electric field $200\mu m$ inside the substrate layer in 13×13 lens [(a) and (b)] and 7×13 lens [(d) and (e)] (color map: normalized). 2–D electric field along the beam–port curve depicting the field spillover at multiple DOAs for (c) 13×13 lens and (f) 7×13 lens.

Note that except for the non–ideal Rotman lens and the RF switch matrix, the remainder of the model in Fig. 1 remains ideal. This assumption is valid since L RF–chains are separated from the Rotman len's beam–ports and the losses for all UE data streams remain the same.

III. Results and Discussion

A. EM and Numerical Results

We excite the array ports of the lens by phase ramped power signals representing multiple DOAs hitting the ULA along the azimuth plane. *Two* distinct scenarios are presented in Fig. 3. The first two columns in Fig. 3 show the simulated normalized E-field 2-D plot on the 13×13 and 7×13 lens substrates, while 1-D contours of E-field recorded at the edges of the beam–ports are compared in the third column. Two rows in Fig. 3 represent two DOA cases, the best and the worst, respectively. The first case corresponds to the incoming EM wave propagating from a transmitting source (or a dominant path scatterer) which is assumed to be located at array broadside direction i.e $\phi = 0°$. It is evident from Fig. 3(a) that the *maximum* power is converged at the central beam–port, i.e. port 7 in 13×13 lens, while a portion of the power is *spilled* to the neighboring ports. Similar spillover is observed in Fig. 3(b) for a 7×13 lens but the field distribution is confined to less number of beam–ports. In other words, the number of ports capturing the *unwanted* fields is higher in 13×13 lens compared to that of 7×13 lens. Looking closely at Fig. 3(c) reveals that the amount of field converged at beam–port 8 in 13×13 lens is no longer seen because of the absence of a port at the same physical location in 7×13 lens. We also notice that as the incoming wave angle ϕ deviates from the broad side direction, two other physical anomalies in the Rotman lens start to dominate. First, an *un-equal* spillover profile over the beam–ports, which is evident from Fig. 3(d) and (e), where the E-field distributes severely in the corner ports. Secondly, for DOA at $\phi = 50°$, field reflections and re-convergences within the lens's body occurs, as evident by Fig. 3(d) and (e). Here, the targeted beam–port was port 13 in 13×13 lens, while a significant amount of unwanted fields were produced at port 1. Same behavior is noticed in 7×13 lens. *These two trends are not significant at broadside-like angles, because the lens in inherently designed to give the best possible E-field convergence operation at $\phi = 0°$.* This inherent physical phenomenon can excite the beam–ports located symmetrically opposite to the beam–port intended by the incoming wave at a specific DOA. The set of results in Fig. 3 highlights a major limitation of the Rotman lens operating as a mm-wave beamformer, and demonstrates the fact that the EM focusing is *more accurate* towards the broadside excitation angles. Let us now consider the separate beam–

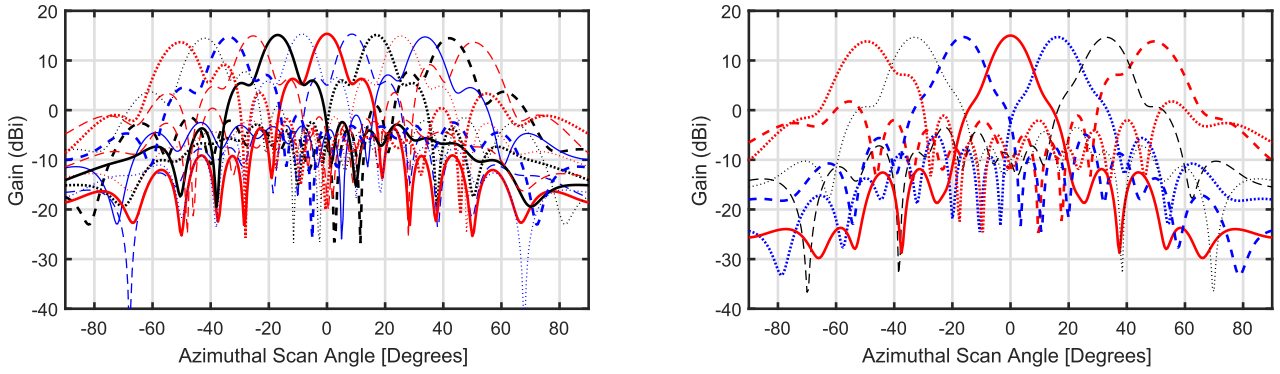

Fig. 4. Simulated far–field realized gain patterns of ULA corresponding to the beam–port excitation of (a) 13×13 lens and (b) 7×13 lens.

port excitations of 7×13 and 13×13 lenses, both connected to the ULA. When the central beam–port is excited in any of the lens, beam projection is expected to be in broad side direction. When any other port is excited, we expect beam projections to be tilted towards a particular ϕ. This is verified by CST Microwave and Design studio co-simulation far-field results. At a uniform excitation level, beam scanning from -50° to $+50^\circ$ is presented in Fig. 4(a) and (b). Beam forming capabilities of both 7×13 and 13×13 lens are evident from the results. We note that even with the same geometrical structure of lens's array ports and ULA, far–field results generated using 7×13 and 13×13 lenses are different. Beams formed with 7×13 lens depicts a consistent thorough sector coverage with high directivity and low inter–beam spacing. On the other hand, beams formed with 7×13 lens are also highly directive but have low-power coverage areas as well between two neighboring beams. For a mm-wave MIMO cellular system, coverage with high resolution is not necessarily required in a given sector. An engineering trade-off in this case can be - *the minimum number of beam–ports required in a Rotman lens that ensures beam coverage resolution is in line with the channel's dominant DOA conditions.* Due to aforementioned anomalies within the Rotman lens's structure, we also note that the gain value at ϕ = $\pm50^\circ$ is lower than the one at ϕ = 0°. A gain decay pattern in visible from Fig. 4 which is non-linear.

B. Sum Spectral Efficiency Results

The impact of RF switch removal and beam–port decimation on the per–terminal MRC SINR and sum spectral efficiency are investigated in this sub–section. Considering the double–direction description in (2), we assume a sector radius of $R_{\text{sector}} = 100$ m. For all the consecutive results, the number of terminals is considered to be seven, with 13 ULA elements at the BS. We assume that the DOAs from a given terminal arrive at the BS via a net azimuthal angular spread of 70°, within which N_{P} = 4 MPCs exist, either in clustered or distinct fashion. In Fig. 5, the SINR of a user terminal is expressed in the form of a cumulative distribution function (CDF), at signal–to–noise–ratio (SNR) = 5 dB, which is generated by considering 10000 independent ensemble realizations of the small–scale fading, each with a unique complementary large–scale fading random variable depending on the link distance and other parameters. Note that the path–loss exponent is considered to be 3.4 and the shadow fading standard deviation is 6 dB. Also note that the case of 13 RF chains with the perfect lens and RF switch operation is considered as a performance benchmark, to compare the imperfections in the lens and RF switching stages of the system. Three trends can be observed from Fig. 5. Firstly, a drastic decrease in the per–terminal SINR can be seen when decreasing the number of active RF chains from 13 to 7. Across all CDF values, a loss of 4.5 dB SINR can be seen due to the loss in multi–path diversity, since all active MPCs do not participate/contribute to recover the terminal data stream, due to lack of active spatial degrees of freedom via low RF chain numbers. Secondly, the imperfections in the RF switch cause a greater loss in the MRC SINR in comparison to the imperfections in the RF lens (comparing the dotted curve with the dashed). This indicates that from a system performance viewpoint, the impact of imperfect beam selection is highly pronounced on the resulting performance. This is later used to motivate its omission. Thirdly, a 4 dB loss in the MRC SINR is observed in the worst–case of imperfect RF lens and switch relative to the case where perfect lens and switch is assumed. If the RF switching network is kept for adaptive beam selection, this comparison yields the performance of the system in practice. More fundamentally, the outage MRC SINR at CDF = 0.05 (5%) has a lower difference due to lower signal power maximization by MRC relative to the peak SINR at CDF = 0.95. To the best of the authors' knowledge, this is the first result to demonstrate the impact of imperfect EM design of the analog beamformer on the system performance.

The result in Fig. 6 depicts the MRC SINR CDF with beam–port decimation and the removal of RF switching, as a consequence. Relative to the 13×13 perfect RF lens and switch case, the 7×13 case with perfect RF lens and no switch leads to a 5 dB MRC SINR loss across all CDF values. This loss is attributed to direct downconversion from the Rotman lens beam–ports to RF chain inputs without any optimization/selection of the best RF paths (as would be the

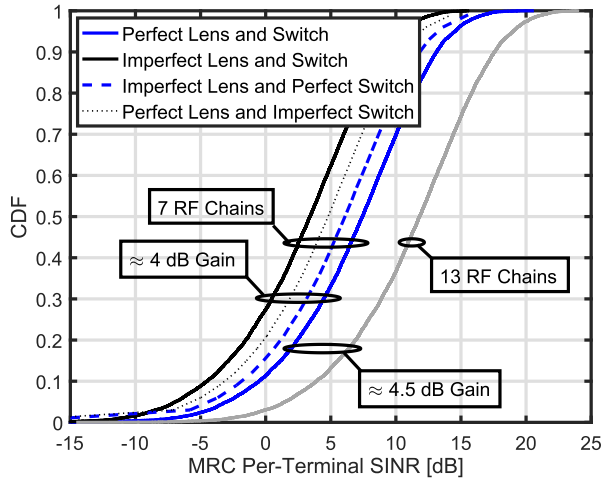

Fig. 5. MRC SINR of a random user terminal at an operating SNR = 5 dB.

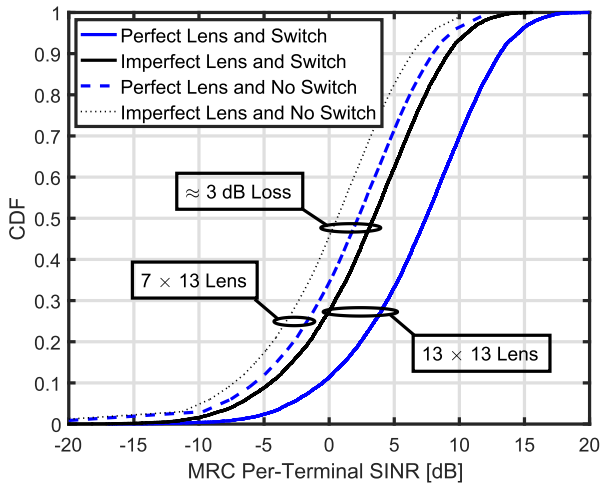

Fig. 6. MRC SINR with and without RF switching at SNR = 5 dB.

case for performance with RF switching). A further loss is incurred when considering the lens imperfections with beam–port decimation due to fundamental impairment of focusing aberrations, and electric field spillover. Overall, the loss of desired signal power and RF beam selection capabilities leads to a decrease in the SINR, however on the positive side, such an approach drastically reduces the implementation complexity of hybrid beamforming systems at mmWave frequencies.

IV. Conclusion

An aggressive hardware reduction approach for mmWave MIMO hybrid architecture is presented, discussed and results are evaluated. The system model for MU–MIMO uplink with 7 user terminals is presented with exact mathematical descriptions. Ideal blocks of beamforming and beam selection networks are replaced with realistic models that involve an accurate estimation of physical impairments. Our investigations show that by decreasing the number of beam–ports in a Rotman lens based hybrid MIMO architecture, the interference profile can be reduced. In addition, removal of an entire beam selection stage is practically viable. The extension of similar port dissimulation principle with other SP techniques is one of the future directions.

V. Acknowledgments

This work was supported by the EPSRC, U.K., under grant EP/P000673/1 and grant EP/EN02039/1.

References

[1] M. Shafi, *et al.*, "5G: A tutorial overview of standards, trials, challenges, deployment, and practice," *IEEE J. Sel. Areas Commun.*, vol. 35, no. 6, pp. 1201–1221, Jun. 2017.

[2] E. G. Larsson, T. L. Marzetta, H. Q. Ngo, and H. Yang, "Antenna count for massive MIMO: 1.9 GHz versus 60 GHz," *IEEE Commun. Mag.*, vol. 56, no. 9, pp. 132–137, Sep. 2018.

[3] W. Hong, *et al.*, "Multibeam antenna technologies for 5G wireless communications," *IEEE Trans. Antennas and Propag.*, vol. 65, no. 12, pp. 6231–6249, Dec. 2017.

[4] A. M. Sayeed and J. Brady, "Beamspace MIMO channel modeling and measurement: Methodology and results at 28 GHz," in *Proc. IEEE GLOBECOM (Workshops)*, Washington, DC, Dec. 2016, pp. 1-6.

[5] R. Mendes-Rial, C. Rusu, N. Gonzalez-Prelcic, A. Alkhateeb, and R. W. Heath Jr., "Hybrid MIMO architectures for millimeter wave communications: Phase shifters or switches?," *IEEE Access*, vol. 4, pp. 247–267, Jan. 2016.

[6] T. Kwon, Y.-G. Lim, B-W. Min and C.-B. Chae, "RF lens-embedded massive MIMO systems: Fabrication issues and codebook design," *IEEE Trans. Microw. Theory Tech.*, vol. 64, no. 7, pp. 2256–2271, Jul. 2016.

[7] Y. Zeng, L. Yang, and R. Zhang, "Multi-user millimeter-wave MIMO with full-dimensional lens antenna arrays," *IEEE Trans. Wireless Commun.*, vol. 17, no. 4, pp. 2800–2814, Apr. 2018.

[8] Y. Gao, M. Khaliel, F. Zheng, and T. Kaiser, "Rotman lens based hybrid analog-digital beamforming in massive MIMO systems: Array architectures, beam selection algorithms and experiments," *IEEE Trans. Veh. Technol.*, vol. 66, no. 10, pp. 9134–9148, Oct. 2017.

[9] H. Tataria, M. Matthaiou, P. J. Smith, G. C. Alexandropoulos, and V. F. Fusco, "Uplink interference analysis with RF switching for lens-based millimeter-wave systems," in *Proc. IEEE ICC*, May 2018, pp. 1-7.

[10] A. Darvazehban, O. Manoochehri, M. A. Salari, P. Dehkhoda and A. Tavakoli, "Ultra-wideband scanning antenna array with Rotman lens," *IEEE Trans. Microw. Theory Tech.*, vol. 65, no. 9, pp. 3435–3442, Feb. 2018.

[11] M. A. B. Abbasi, V. F. Fusco, H. Tataria and M. Matthaiou, Constant-ϵ_r lens beamformer for low-complexity millimeter-wave hybrid MIMO," *IEEE Trans. Microw. Theory Tech.*, Jun. 2019.

[12] M. A. B. Abbasi, H. Tataria, V. F. Fusco and M. Matthaiou, "On the impact of spillover losses in 28 GHz Rotman lens arrays for 5G applications," in *Proc. IEEE IMWS-5G*, Dublin, 2018, pp. 1-3.

[13] R. C. Hansen, "Design trades for Rotman lenses," *IEEE Trans. Antennas Propag.*, vol. 39, no. 4, pp. 464–472, 1991.

[14] W. Rotman and R. F. Turner, "Wide angle microwave lens for line source applications," *IEEE Trans. Antennas Propag.*, vol. 11, no. 6, pp. 623–632, Nov. 1963.

[15] Wi Sang-Hyuk, *et al.*, "Package- level integrated antennas based on LTCC technology," *IEEE Trans. Antennas Propag.*, vol. 54, no. 8, pp. 2190–2197, Aug. 2006.

[16] A. C. Bunea, D. Neculoiu, M. Lahti and T. Vaha-Heikkila, "Stripline-fed LTCC microstrip patch antenna for 35 GHz applications," in *Proc. International Semiconductor Conference*, 2014, pp. 167–170.

[17] CST Studio Suite by *Computer Simulation Technology*, Darmstadt, Germany, 2018. [Online] Available: http://www.cst.com

[18] M. A. Hassanien, M. Jenning and D. Plettemeier, "Beam steering system using rotman lens for 5G applications at 28 GHz," in *Proc. IEEE ISPA USNC/URSI*, San Diego, CA, July 2017, pp. 2091-2092.

[19] A. Darvazehban, O. Manoochehri, M. A. Salari, P. Dehkhoda and A. Tavakoli, "Ultra-wideband scanning antenna array with Rotman lens," *IEEE Trans. Microw. Theoy Techn.*, vol. 65, no. 9, pp. 3435–3442, Sept. 2017.